36th ERF Paper No. 052

Rotorcraft Simulation Renovation through System Identification

Linghai Lu, Gareth D Padfield, Mark White, Philip Perfect*
Flight Science & Technology, School of Engineering
University of Liverpool, Liverpool, L69 3GH, UK
*Email: Linghai@liv.ac.uk

High fidelity modelling and simulation are prerequisites for robust aircraft design and development, including performance and handling qualities, control system design, and aircraft dynamic loads analysis. Accurate modelling of flight dynamics is also one of the key elements in the creation of a realistic simulation environment, where the quantification of fidelity underpins the confidence required for providing an economic, reliable, and safe test bed for pilot training and certification. The techniques of system identification provide a systematic framework for 'renovating' a physics-based simulation model derived from first principles and aircraft design data. In this paper we adopt a frequency domain approach for model renovation and fidelity improvement of a baseline FLIGHTLAB Bell412 helicopter developed at the University of Liverpool. The structure of the model is built up from frequency-sweep response data from flight test. Predictability is based on responses to multi-step control inputs. The techniques have been used to generate one, three, and six degree-of-freedom linear models, and their derivatives and predictability are compared to evaluate and augment the fidelity of the FLIGHTLAB model. The renovation process thus involves augmenting the simulation model based on the identified parameters. First results are reported within the context of the rotorcraft simulation fidelity project, *Lifting Standards*, involving collaboration with the Flight Research Laboratory (NRC, Ottawa), supported with flight testing on the ASRA research helicopter.

NOMENCLATURE

a_x, a_y, a_z = accelerations in body axes (longitudinal, lateral, vertical), ft/s^2
A, B, C, D = state-space matrices in linear aircraft dynamics
$K_{\delta_{lat}}$ = gain between the pilot stick and rotor swashplate
L, M, N = external moments about the centre of gravity (roll, pitch, and yaw)
$L_{\beta_{1s}}$ = effective flap stiffness
n_{TF}, n_ω = number of individual input-output pairs and number of frequency points selected in the fitting
p, q, r = perturbation angular velocities (roll, pitch, and yaw), deg/s
T, $\hat{T}_c$ = the updated frequency-response estimate and the desired transfer function
u, v, w = perturbation translational velocities (longitudinal, lateral, vertical), ft/s
W_g, W_p, W_r = weighting functions for cost function
X, Y, Z = external forces on the centre of gravity (longitudinal, lateral, vertical)
α, β = angle of attack and sideslip angle, deg
β_{1s} = lateral flapping angle, deg
δ_{col}, δ_{lat} = control inputs (collective and lateral), in
δ_{lon}, δ_{ped} = control inputs (longitudinal and pedal), in
θ, ϕ = fuselage attitude angles (pitch and roll), deg
θ_{1c} = lateral cyclic angle, deg
τ_{eq} = equivalent time delay, s
τ_f = rotor flap time constant, s
$\tau_{\delta_{lat}}$ = time delay between pilot stick and rotor , s

INTRODUCTION

System identification (SI) is a systematic and efficient approach to extracting aircraft dynamics models from flight test data. Such models have been extensively used to support both fundamental and applied research into aircraft behaviour in a number of key areas [1-7]. These techniques play two main roles during the development of a new aircraft [5;8;9]. The first is to validate and improve the accuracy and predictability of a theoretical model – the renovation process - by comparing the identified model structure and parameters from simulation and flight test data. SI can improve the understanding of aircraft flight behaviour and the identified derivatives can be used to determine correction factors to improve the fidelity of physics-based simulation models [5;6]. Secondly, in many applications, the results of SI are expressed in state-space form in terms of stability and control derivatives or in the transfer-function form such as low-order equivalent system (LOES) model. When interpreted appropriately, these values can be used to demonstrate compliance with requirement specification (e.g. handling qualities [10]), and support model renovation. Such models can also form the basis of full flight envelope models using the stitching process, described by Zivan and Tischler in [11].

There is extensive literature concerning SI applied to fixed-wing aircraft [12-15]. Rotary-wing aircraft present a greater challenge but important strides have been taken over the last two decades [5;6;8;9;16]. Rotorcraft data often exhibit low signal-to-noise ratio because of the high vibration environment. The all-important air data measurements are strongly affected by rotor wake and fuselage flow field effects, particularly at low speed. Moreover, higher-order structures can be required to model the dynamic coupling between components, for

example, the rotor, power plant/transmission system and fuselage. Rotorcraft system identification is not yet a mature discipline.

The research described in this paper uses the SI toolbox, Comprehensive System Identification from Frequency Responses (CIFER®), developed initially at the Ames Research Center [5]. The focus is a systematic approach to simulation fidelity and renovation, including the development of predicted and perceived metrics; the Bell 412 helicopter model developed in FLIGHTLAB by the University of Liverpool (UoL) is one of the baseline research tools used [17] [18]. Results from SI are integral to this fidelity project and complementary to techniques aimed at overall pilot-vehicle fidelity assessment [7].

The paper first presents comparisons between responses from flight-test and FLIGHTLAB simulation, driven by the multi-step control inputs in the time domain, and by the frequency-sweep inputs in the frequency domain. Secondly, comparisons of the stability and control derivatives computed from CIFER® and FLIGHTLAB perturbation analysis are evaluated with the extracted models of increasing degrees of freedom (DoF) - starting with one DoF attitude rate response, then moving to 3 DoF pitch/heave/surge and roll/yaw/sway motion and, finally, 6 DoF coupled longitudinal/lateral motion. The paper presents the first results from a model renovation process. Conclusions from this preliminary investigation and the directions of future work complete this paper.

ELEMENTS OF SIMULATION FIDELITY

The ability to replicate real aircraft behaviour in a realistic environment is the kernel of good flight simulation, in which students can train to operate aircraft proficiently and safely or designers can evaluate and optimise concepts. Regulatory authorities have produced documents such as JAR-STD 1H [19] and FAA AC120-63 [20] to describe the qualification criteria and procedure for rotorcraft flight training simulators. These documents detail the component fidelity required to achieve a "fit for purpose" approval. Such criteria are formulated by using "tolerances", defined as acceptable differences between the simulation and flight test, typically ±10% for flight model tolerances [18].

JAR-STD 1H describes a four-level fidelity qualification (A, B, C, and D), Level D being the highest and strongly representative of real flight. A Level D simulator can be used to replace most of the conversion and recurrent flight hours. However, Level D standards for model accuracy mean that it is usually necessary to modify parameters and components of the simulation model through a process of both physical and non-physical tuning and adjustment. Efforts have been made to establish an engineering basis for this tuning process [5;21;22]. For example, Tischler [5] proposed the idea of boundaries on maximum unnoticeable added dynamics (MUAD) as part of the FAA level D simulation fidelity criteria. If the applied boundary is violated, then the pilot is likely to be aware of a deviation in the simulator response characteristics from the real aircraft. The proposed criteria also have been used in helicopter simulation validation research activities [22]. GARTEUR Action Group HC-AG12 [21] conducted sensitivity analyses using the JAR simulator standards, including correlation of handling qualities and fidelity metrics, revealing shortcomings. In particular, the AG showed that the relationship between fidelity and the tolerances prescribed by JAR-STD 1H is sensitive to the form and duration of manoeuvres; another result was that models of the aircraft-pilot 'system' offer potential as a basis for overall fidelity. Experience highlighted in the GARTEUR HC-AG12 study showed that, in most areas, 80% "fidelity" should be achievable with physical modelling but that the remaining 20% requires artificial tuning; this last 20% is critical for acceptance.

Rationalisation of simulator qualification standards, either fixed wing or rotary wing, must address the underlying question of the suitability of the criteria for specifying each of the component parts, and the overall fidelity of the simulator. What is required is an objective means for this overall assessment, to complement perceived fidelity and the predicted component fidelity. Developing such assessment methods is the theme of a project involving collaboration between the UoL and the National Research Council (NRC, Canada). The initial phase of this project involved the collection of flight test measurements on the Bell 412 ASRA (advanced systems research aircraft – Figure 1) for use as benchmark data. Using a FLIGHTLAB Bell412 (F-B412) model [17], the predictive fidelity of the flight model has been assessed against the benchmark data. The flight test manoeuvres were "re-run" within the research simulation facilities at UoL to examine the fidelity of the overall simulation environment. The data from both the UoL simulation and flight trials are being used to derive a set of fidelity metrics for rotorcraft simulation.

Figure 1 The NRC ASRA Research Aircraft

The work reported in this paper forms part of this on-going project, providing an alternative approach to the model fidelity assessment and renovation based on SI in the frequency domain. The research consists of four stages. The first focuses on comparing flight-test responses and those from the F-B412 simulation; discrepancies in the time and frequency domain are used to highlight the deficiencies existing in the simulation. Secondly, SI is used to derive and compare the key parameter values for first-order (short term) attitude response models. These LOES models can then used to evaluate fidelity in terms of flight handling qualities [13] and also as a reference for higher-order model fidelity. Thirdly, SI is used to derive

stability and control derivatives for both 3 DoF and 6 DoF state-space model structures from both flight test and simulation data. The comparison of these derivatives can provide a deep insight into the accuracy of the F-B412 model. Finally, SI can be used to develop hybrid models that account for rotor flap, lead-lag, and coning-inflow dynamics [5]. The results based on this model structure aid understanding of the higher order dynamic couplings that impact piloting and flight performance. The key results from the exploratory work conducted to date are described in this paper.

SYSTEM IDENTIFICAITON METHODOLOGY

A. CIFER summarised

The software CIFER® is the processing and analysis tool used in this research (Figure 2). Guidelines for designing a frequency sweep control input, conducting a flight test, and generating a high-quality time-history database, outlined in Figure 2, are described in Refs. [4;5]. The response time histories are transformed into the frequency domain with the chirp z-transform logarithm and then processed with the 'input correlation reduction' and 'windowing' algorithms. This can help to reduce the possible present effects of multiple, partially correlated controls for a given recorded manoeuvre and to achieve a high-quality frequency-response database with enough bandwidth and low random error. The final frequency responses are used for transfer-function and state-space model parameter identification

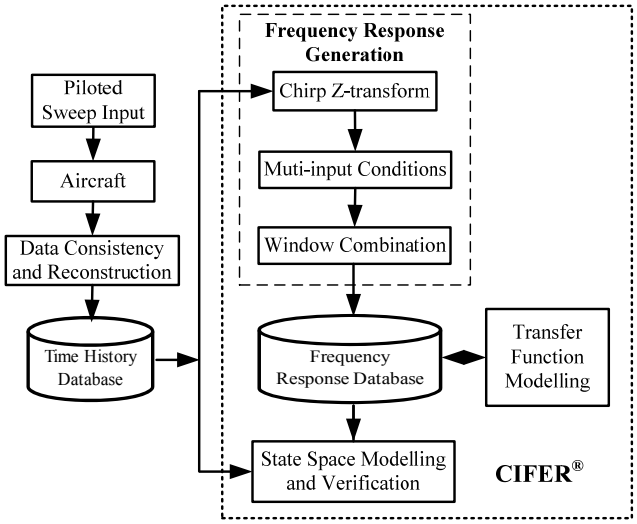

Figure 2 Flow chart of the CIFER® process

The cost-function used for parameter optimisation in CIFER® can be formulated as follows,

$$J = \sum_{l=1}^{n_{TF}} \{ \frac{20}{n_\omega} \sum_{\omega_1}^{\omega_{n_\omega}} W_r [W_g (\left|\hat{T}_c\right| - \left|T\right|^2) + W_p (\angle \hat{T}_c - \angle T)^2] \} \qquad (1)$$

where n_{TF} is the number of individual input-output pairs, n_ω is the number of frequency points selected in the fitting frequency range [ω_1, ω_{n_ω}], which is likely to be different for each pair. The unknown parameters in Eq. (1) are identified based on minimizing the errors of magnitude ($\left|\ \right|$) and phase ($\angle$) between the desired transfer function (T) and the updated frequency-response estimate ($\hat{T}_c$). The three terms W_r, W_g, and W_p are weighting functions providing the user a control over the data selection.

During the identification procedure, the model structure is refined based on Cramér-Rao (CR) bounds for the individual identified parameters. The CR inequality, defined as the minimum expected standard deviation for a given parameter estimate, provides the theoretical accuracy based on correlation. The recommend maximum value for the CR bound in CIFER® is 20% of the parameter value. If the CR value exceeds this, it can reflect two problems: insensitivity of an identified parameter to the minimisation process and/or correlation between different parameters. The parameters with high CR values are rejected and the optimization process then repeats again, based on the refined model structure. If the new cost function in Eq. (1) shows a defined reduction, then the refined model structure is used; otherwise, the rejected parameter has to be retained and the cycle repeated. The process is systematic, but because, on the one hand, the model is an approximant to a nonlinear time varying reality and, on the other, the test data is less than perfect (containing both measurement and process noise), the search for the optimum identified model is a creative 'art' as well as a rational 'science'. This dual aspect has bedevilled SI since its inception, and in this paper the authors highlight areas where this duality comes to the fore.

B. Structure definition for system identification

The state-space six DoF model structure used for identification in this paper is given in (2),

$$\begin{aligned} \dot{\boldsymbol{x}} &= \boldsymbol{A}\boldsymbol{x} + \boldsymbol{B}\boldsymbol{u}(t-\boldsymbol{\tau}) \\ \boldsymbol{y} &= \boldsymbol{C}\boldsymbol{x} \end{aligned} \qquad (2)$$

where

$$\boldsymbol{x} = \begin{bmatrix} u \\ v \\ w \\ p \\ q \\ r \\ \phi \\ \theta \end{bmatrix} \qquad \boldsymbol{u} = \begin{bmatrix} \delta_{lat} \\ \delta_{lon} \\ \delta_{ped} \\ \delta_{col} \end{bmatrix} \qquad \boldsymbol{y} = \begin{bmatrix} \dot{u} \\ \dot{v} \\ \dot{w} \\ p \\ q \\ r \\ a_x \\ a_y \\ a_z \end{bmatrix} \qquad (3)$$

The variable ($\boldsymbol{\tau}$) is included in Eq. (2) to account for unmodelled higher-order dynamics such as the rotor flap response, and the control system/actuator delays/lags [1;5]. The physical meaning of the symbols in Eq. (3) follows the usual convention in flight dynamics – u, v, and w are the aircraft perturbation translational velocities in the body-frame, p, q, and r are aircraft perturbation rotational velocities in the body-frame, and ϕ and θ are Euler roll and pitch angles. The

vector ***u*** consists of the four helicopter controls. a_x, a_y, and a_z in the measurement output vector (***y***) are inertial accelerations in the body frame. The first-order derivatives of *u*, *v*, and *w* are used in this paper because this selection normally leads to higher coherence between the related input-out pairs [5].

The accuracy of system identification depends on the quality of the recorded data and consequently requires the aircraft instrumentation system to provide reliable and consistent information for identification [4;5;16]. The data from three flight conditions at true air speeds (TAS) 35, 65, and 95 kts are selected for identification in this paper.

C. Open-loop and closed-loop identification

The F-B412 model consists of a four-bladed rigid, articulated, blade element main rotor system with flap and lag degrees of freedom. Rotor inflow is modelled using the Peters-He finite-state dynamic inflow model. The tail rotor is modelled using the Bailey method [16]. A table look-up method is used to model the fuselage aerodynamic force and moment coefficients as functions of the angles of attack and sideslip. Left-side and right-side horizontal stabilisers are modelled independently using lifting surface theory, with each stabiliser having independent initial incidence settings. Each stabiliser is attached to a spring-loaded tube, allowing the incidence to change in flight according to the aerodynamic pitching moment experienced by the surface. The vertical fin is likewise modelled using lifting surface theory. Engine dynamics were derived from an NRC linear state-space model of the engine-governor-rotor system. The response of this linear model was used to tune the FLIGHTLAB 'simple engine' component to give a well-matched, second order response. The simple engine model acts as an engine governor, commanding torque to hold the rotor speed constant.

The FLIGHTLAB simulation environment provides different approaches to linearization, based on either perturbation or identification techniques. The accuracy of the results is sensitive to factors such as perturbation size, model structure as well as nonlinear elements, for example in the control system or the interactional aerodynamics [5]. System identification also provides a methodology to derive linear models from a nonlinear simulation with piloted or mechanised frequency-sweep inputs, akin to flight test. However, when the aircraft is unstable, this can present a problem. One approach to overcome the divergent problems of an unstable system makes use of the measurements for bare-airframe + stability and control augmentation system (SCAS) configuration to identify the bare airframe parameters. With this structure, the inputs for SI are the measured control surface values (rather than the cockpit inceptor positions); Figure 3 illustrates the scheme, which is used in this paper to generate the frequency response comparisons in the next section. For the identification of stability and control parameters, the results of this technique have been mixed and are only shown in this paper for the low order model.

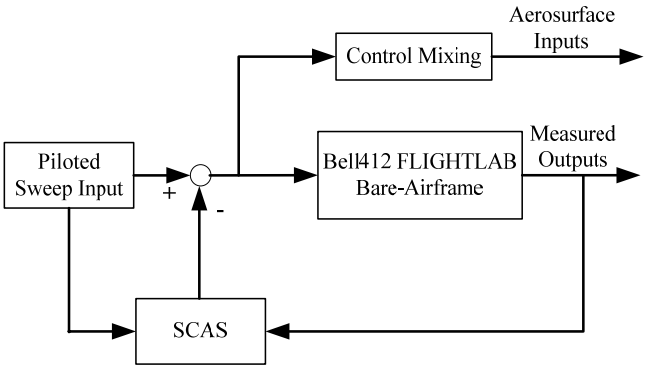

Figure 3 Scheme of closed-loop simulation in FLIGHTLAB [5]

Frequency sweeps were performed at a number of different flight conditions. The majority of the results presented will be at true air speeds (TAS) of 35, 65, and 95 kts. The actual flight conditions and aircraft configurations were matched as close as possible, in terms of inertias, c.g. position, wind, altitude, and temperature.

Of the 52 available input-output frequency response pairs (e.g. $p/\delta_{lat}, \dot{w}/\delta_{col}, \theta/\delta_{lon}, a_y/\delta_{ped}$) generated, only 14 satisfied the basic $J < 100$ *criterion*. The frequency-range selection has two primary drivers. The first is to select a range over which the coherence is above 0.6 (recommended in [5]). Coherence can suffer from noise contamination in the measurement outputs, nonlinearities that cannot be modelled by the describing function, and process noise (e.g. unknown or unmeasured inputs). The second is the importance of appropriate modelling of dynamics in the application frequency range. For example, the range needs to exclude the rotor response above about 10 rad/s. The frequency ranges over which the coherence was greater than 0.6 varied for each pair, or 'response fragment' and *J* could sometimes be reduced by narrowing the frequency range. For example, the value of *J* for the fragment of p/δ_{lon} was reduced to 45 by narrowing the fit range to [0.47, 1.4] rad/s. In the best cases the frequency spanned the whole dynamic range of interest, e.g. p/δ_{lat} where [0.30, 10] rad/s, with $J = 63$. Typical results from the frequency identification are illustrated in Figures 4 and 5.

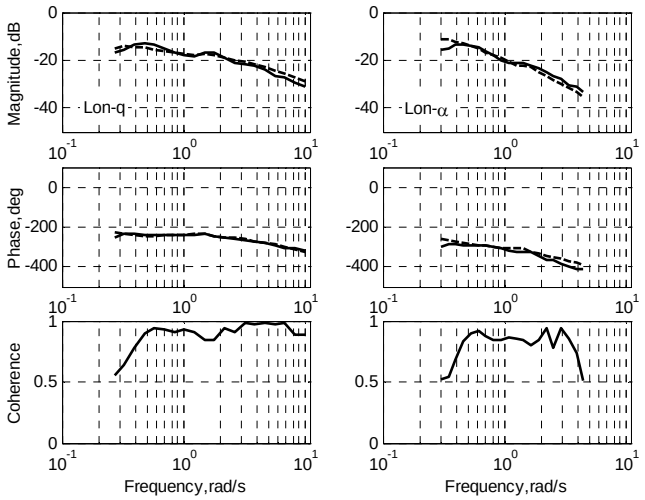

Figure 4 Frequency domain fit for q/δ_{lon} and α/δ_{lon}

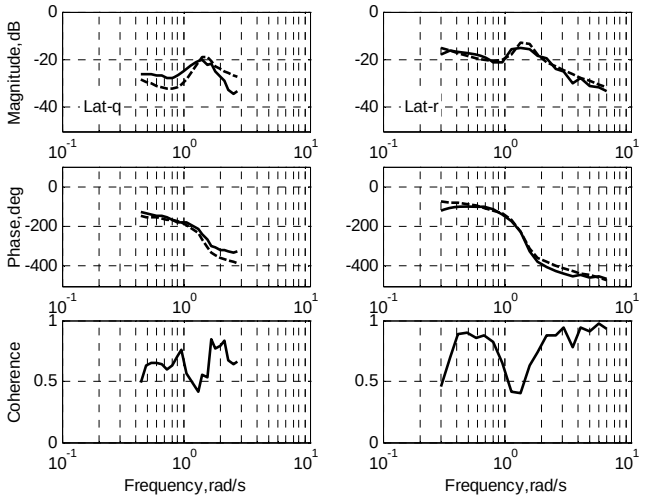

Figure 5 Frequency domain fit for q/δ_{lat} and r/δ_{lat}

The on-axis response in Figure 4 shows a good fit over a wide frequency range – up to 9 rad/s for the pitch rate response to longitudinal cyclic for example. The pitch rate from lateral cyclic response in Figure 5 shows a much poorer fit at low frequency for the gain (indicates a potential problem with estimating 'quasi-steady' coupling derivatives). The dip in coherence around 1.5 rad/s is also seen in the yaw rate from lateral cyclic, highlighting potential identification problems of individual derivatives around the Dutch roll frequency. Selecting fragments of the responses where coherence is high and cost function low can, in principle, be systematically automated, but is also part of the 'hand-crafting' of SI, where prior knowledge can sometimes aid this critical data preparation stage in the SI process.

RESPONSE COMPARISONS F-B412 VS FLIGHT TEST

A. Response comparisons in the time domain

A preliminary validation of the F-B412 model was presented in Ref. [17], showing good on-axis but poorer off-axis response predictions; a sample result is illustrated in Figure 6, showing responses to a longitudinal stick multi-step input (δ_{lon}).

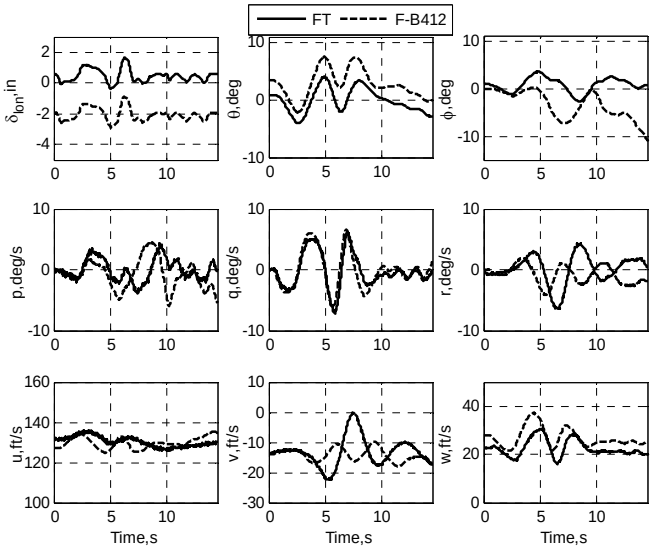

Figure 6 Comparison of flight and simulation responses to a longitudinal stick multi-step (TAS = 80 kts)

There are consistent trim offsets in pitch and heave velocity between flight and simulation. The lateral-directional responses are seen to be under-predicted by the F-B412 model, particularly sideslip and yaw rate. This suggests that stronger yaw moments were generated during the pitch/heave manoeuvre in flight with similar levels of pitch rate and incidence change. These rough comparisons can inform the SI analysis, alongside similar comparisons in the frequency domain.

B. Response comparisons in the frequency domain

Response comparison in the frequency domain provides a reference point for establishing appropriate model structures and evaluating fidelity of the non-linear simulation model [5;22]. For comparison with the flight test data, the rotor control inputs have been transformed to the cockpit inputs for the F-B412, using the control gearings (note that these inputs will not necessarily be the same as the inputs applied in flight). For each of four control channels, typical responses are selected for illustration in Figure 7 and 8 across a frequency range of about 0.2 to 10 rad/s. The on-axis magnitude and phase fits are generally very good with coherence high above 1 rad/s accept for the dip in the lateral response just above this value, previously identified in Figure 5.

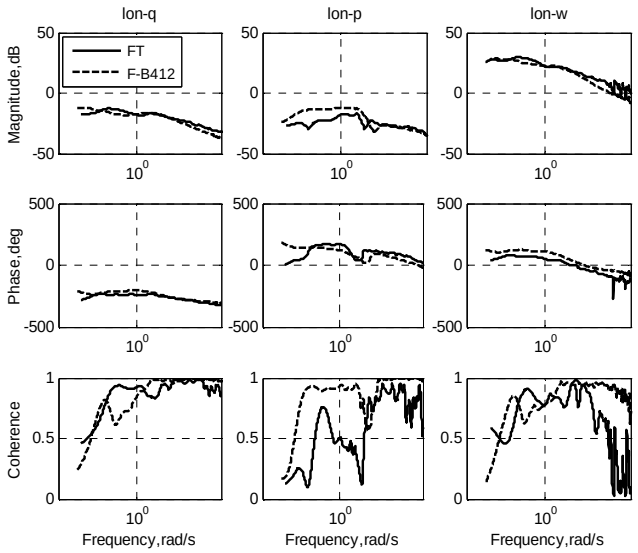

Figure 7 Comparison of responses in the frequency domain (TAS = 95 kts) – longitudinal cyclic sweep

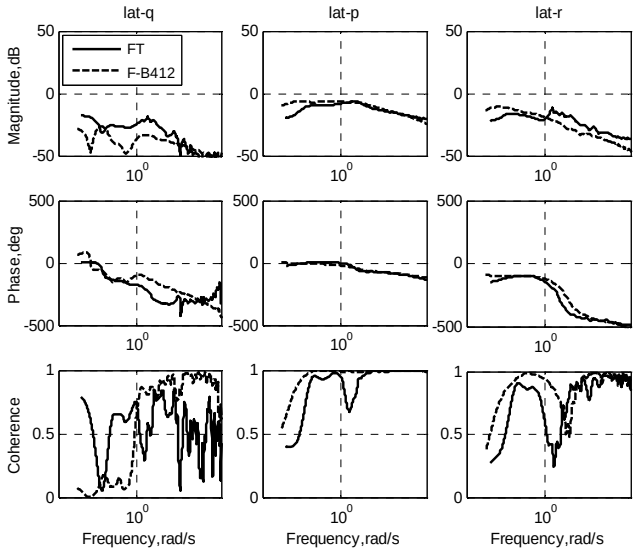

Figure 8 Comparison of responses in the frequency domain (TAS = 95 kts) – lateral cyclic sweep

SYSTEM IDENTIFICATION OF SINGLE-DOF ROLL MOTION

A. Single DOF quasi-steady roll model

A first-order quasi-steady model of rotorcraft roll response to lateral cyclic, with an equivalent time delay, can be described as follows [1;5]:

$$\frac{p}{\delta_{lat}}(s) = \frac{L_{\delta_{lat}} e^{-\tau_{\delta_{lat}} s}}{s - L_p} \tag{4}$$

where $L_{\delta_{Lat}}$ is the roll-control sensitivity, L_p is the roll damping derivative, and $\tau_{\delta_{lat}}$ is the equivalent time delay, modelled from the contribution of the transient rotor response. A typical range for this kind of application is 0.1 to 10 rad/s. The identified parameters from flight test and F-B412 are shown in Table 1 and Table 2, respectively, across the speed range 20-120 kts. In addition, the L_p values are compared with those from the linearised F-B412, using the perturbation approach, in Figure 9.

Table 1 Identified parameters for one DoF roll mode - flight test

Cases	$L_{\delta_{lat}}$	L_p	τ, s	CF.
FT20	0.998	-2.10	0.0636	16.3
FT35	0.951	-2.49	0.0746	11.1
FT65	0.930	-2.04	0.0698	58.7
FT95	0.901	-1.87	0.0672	65.7
FT120	0.917	-1.78	0.0667	110

Table 2 Identified parameters for one DoF roll mode – F-B412

Cases (kts)	$L_{\delta_{lat}}$	L_p	τ, s	CF.
20	0.914	-2.20	0.0544	18.1
35	0.924	-2.45	0.0608	21.4
65	0.927	-2.00	0.0569	9.01
95	0.990	-1.90	0.0529	24.0
120	0.946	-1.87	0.0545	58.7

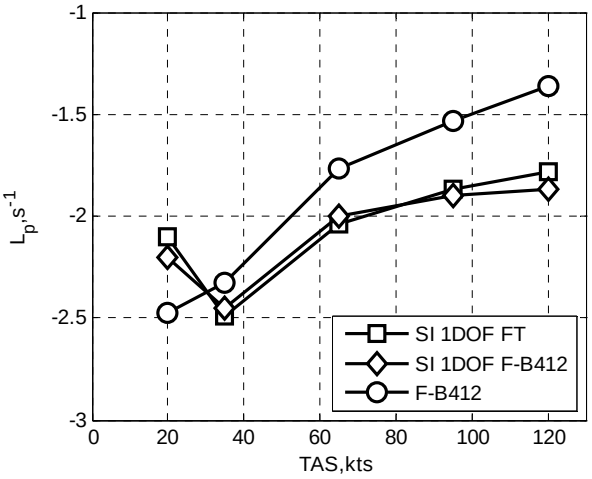

Figure 9 Comparison of L_p values from SI and linearised perturbations

In Table 1, the term FT is the abbreviation for flight test; in Table 2, F-B412 are the FLIGHTLAB results. CF is the cost function. The numerals in the case names relate the different forward speeds.

As shown in Table 1 and Table 2, and more clearly in Figure 9, the identified L_p values both from flight test and F-B412 data are quite close but both differ from the perturbation results, although the trend of reducing damping as forward speed

increases is common to all. In addition, the identified values have converged with low cost function as shown in Table 1 and Table 2 (mostly below 100, as recommended in [5]). The effectiveness of the low cost-function values can be shown by comparison with the flight frequency responses, and assessing against fidelity criteria. Taking the 95 kts case for illustration, the results shown in Figure 10 reflect the good match in terms of magnitude and phase. The good fit can also be observed in the magnitude and phase error functions in Figure 11. Here, 0-dB magnitude and 0-deg phase indicate a perfect match of the flight and simulation results. The dashed curves are the model mismatch boundaries recommended for the highest-fidelity training simulators (FAA Level D) [5]. These boundaries relate limits on MUAD used in fixed-wing handling-qualities criteria. When the magnitude and phase errors are located within these boundaries, the pilot is unlikely to be able to distinguish between the handling qualities from the aircraft and the low-order equivalent system. The results of all five cases lie well within these boundaries and provide a degree of validation of the first-order model of roll response to lateral cyclic and a reference for the multi-degree-of-freedom modelling. Three 'renovation' related questions arising from the comparisons in Figure 9 are – why do the results from flight and nonlinear F-B412 show an slight increase in L_p at low speed; why the subsequent 25% reduction in L_p with increasing speed? Why the larger reduction in L_p from the perturbation method?

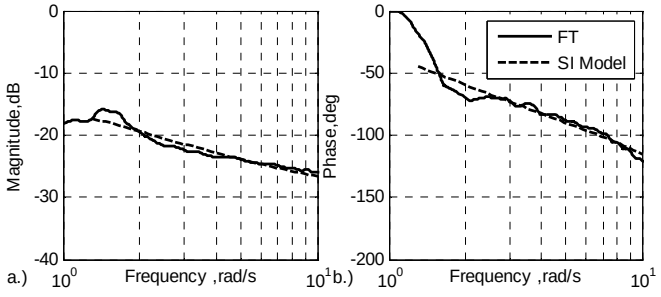

Figure 10 Comparison of response from the identified roll mode with flight test data at TAS = 95 kts

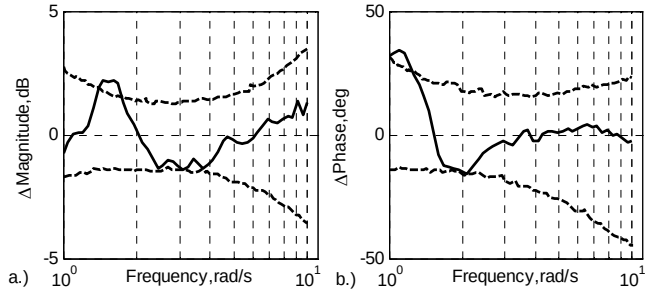

Figure 11 Error functions compared with proposed level D simulation fidelity criteria at TAS = 95 kts

The main sources of roll moment are from the tail rotor, vertical stabiliser and main rotor. As illustrated in Figure 12, the main rotor is the dominant contribution. Ignoring the in-plane load contribution, this has itself two sub-components – one from the hub moment originating from the rotor stiffness or flap hinge offset, and the other from the thrust vector tilt from the centre of gravity [1]. 'Simple' rotor theory suggests that L_p should be fairly constant over the speed range considered. The presence of non-uniform downwash effects in flight and the F-B412 model are the likely cause of this decreasing damping, reducing the lateral flapping in response to the development of aerodynamic hub moments.

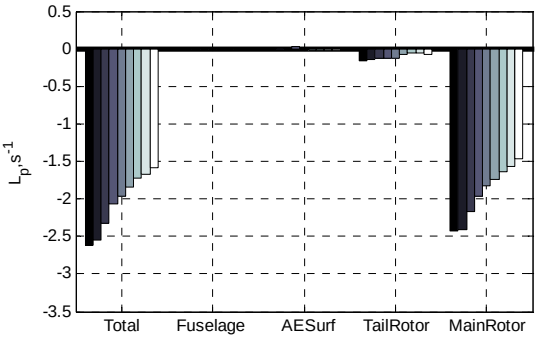

Figure 12 Contributions of components to L_p (shading represents TAS variation from 20 to 100 kts at an increments 10 kts)

The predictive capability of this 1 DoF roll model can be assessed using the multi-step input in Figure 13. The term N-F-B412 in Figure 13 refers to the nonlinear FLIGHTLAB model response. The results from the CIFER model match the flight test data very well, as expected. This validates the on-axis roll response fidelity of the F-B412, as well as demonstrating the effectiveness of including the SCAS to identify a single DoF bare-airframe transfer function.

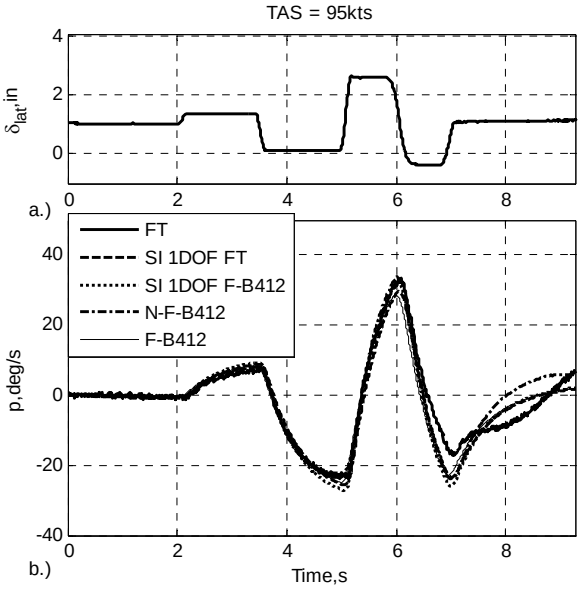

Figure 13 Verification of SI roll mode with flight test data

B. Two DoF rotor-body coupling model

The model in Eq. (4) only accounts for the influence of the quasi-steady rotor response on helicopter flight dynamics. Taking to the next level of complexity, the regressing flap mode can be approximated as follows [5],

$$\tau_f \dot{\beta}_{1s} = -\beta_{1s} + \tau_f p + \theta_{1c} \tag{5}$$

where τ_f is the rotor flap time constant, θ_{1c} is the lateral cyclic deflection, and β_{1s} is the lateral flapping. The induced rolling acceleration can then be expressed as,

$$\dot{p} = L_{\beta_{1s}} \beta_{1s} \tag{6}$$

in which the term $L_{\beta_{1s}}$ is the effective flap stiffness. Treating the linkage/actuator between the pilot stick (δ_{lat}) and the rotor swashplate as a pure gain ($K_{\delta_{lat}}$) and time delay (τ_{lat}), the corresponding relationship can be written as,

$$\theta_{1c} = (K_{\delta_{lat}} e^{-\tau_{lat} s}) \delta_{lat} \tag{7}$$

By combining Eq. (5) with Eq. (7), the roll-rate response to the pilot cockpit stick, or the coupled roll-flap dynamics, can be written in the transfer function form,

$$\frac{p}{\delta_{lat}}(s) = \frac{K_{\delta_{lat}} L_{\beta_{1s}} e^{-\tau_{lat} s}}{\tau_f s^2 + s - \tau_f L_{\beta_{1s}}} \tag{8}$$

If the condition

$$(\tau_f)^2 \ll \left| \frac{1}{L_{\beta_{1s}}} \right| \tag{9}$$

is satisfied, the simpler transfer function shown in Eq. (4), can be used to model the roll response. The equivalent time delay is then,

$$\tau_{\delta_{lat}} = \tau_f + \tau_{lat} \tag{10}$$

and the roll control sensitivity is given as,

$$L_{\delta_{lat}} = K_{\delta_{lat}} L_{\beta_{1s}} \tag{11}$$

The roll damping derivative is then,

$$L_p = \tau_f L_{\beta_{1s}} \tag{12}$$

The SI results, based on Eq. (8), are shown in Table 3. The parameters identified directly are $K_{\delta_{lat}} L_{\beta_{1s}}$, τ_{lat}, τ_f, and $\tau_f L_{\beta_{1s}}$. The term $L_{\beta_{1s}}$ in Table 3 is calculated from the identified values. The relationship between the rotor time constant (τ_f) and the roll-damping derivative L_p ($\tau_f L_{\beta_{1s}}$) is satisfied with the requirement of Eq. (9). The applicability of the SISO model in Eq. (4) is therefore verified. Moreover, the equivalent time delays in Eq. (4), listed in Table 1, closely matches the combined τ_{lat} and τ_f in Table 3.

Table 3 Identified values for rotor-body coupling model

Cases	FT20	FT35	FT65	FT95	FT120
$L_{\beta_{1s}}$	-60.1	-64.3	-88.4	-98.4	-70.0
$K_{\delta_{lat}} L_{\beta_{1s}}$	0.949	0.908	0.914	0.876	0.887
τ_{lat}, s	0.0301	0.0404	0.0510	0.0485	0.0418
τ_f, s	0.0333	0.0412	0.0250	0.0184	0.0247
$L_{\beta_{1s}} \tau_f$	-2.00	-2.65	-2.35	-1.87	-1.80
CF.	15.4	32.8	78.0	66.2	111

The identified rotor flap stiffness are located in typical range of $60 < -L_{\beta_{1s}} < 100$. Mover, the analysis, based on Eq. (9),suggests that Eq. (4) is generally accurate over the frequency range of interest (0.1 – 10 rad/s) for the F-B412 roll response to cyclic, as result confirmed by the fairly linear behaviour of the frequency response in the upper range of frequencies in Fig. 9.

SYSTEM IDENTIFICATION WITH THREE AND SIX DoF MODELS

The 6 DoF rotorcraft model can be divided into two 3 DoF sub-models in Eq. (2) representing the sway/roll//yaw and surge/heave/pitch dynamics, with couplings ignored. The transient rotor flap response is modelled as a pure time delay on the control inputs. The SI results for the 3 DoF and 6 DoF models, across the speed range 35-95 kts, are given in table form in Appendix A and graphical form in Figure 14 and Figure 15. The results are compared with the perturbation results from the F-B412 model.

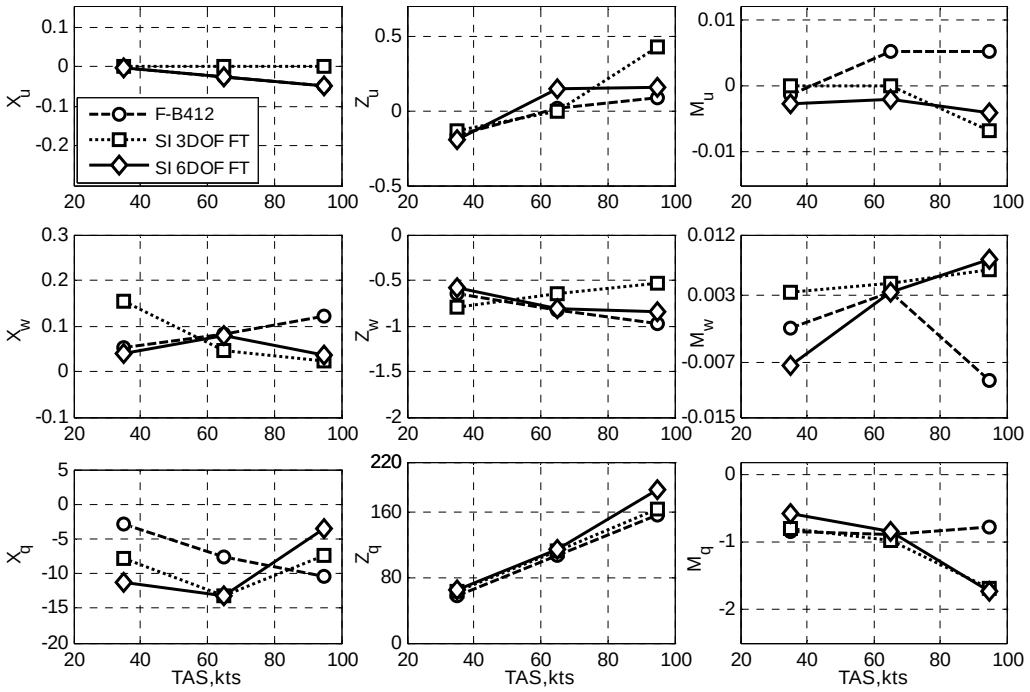

Figure 14 Comparison of longitudinal stability derivatives from 3DOF and 6DOF SI FT and FLIGHTLAB perturbation

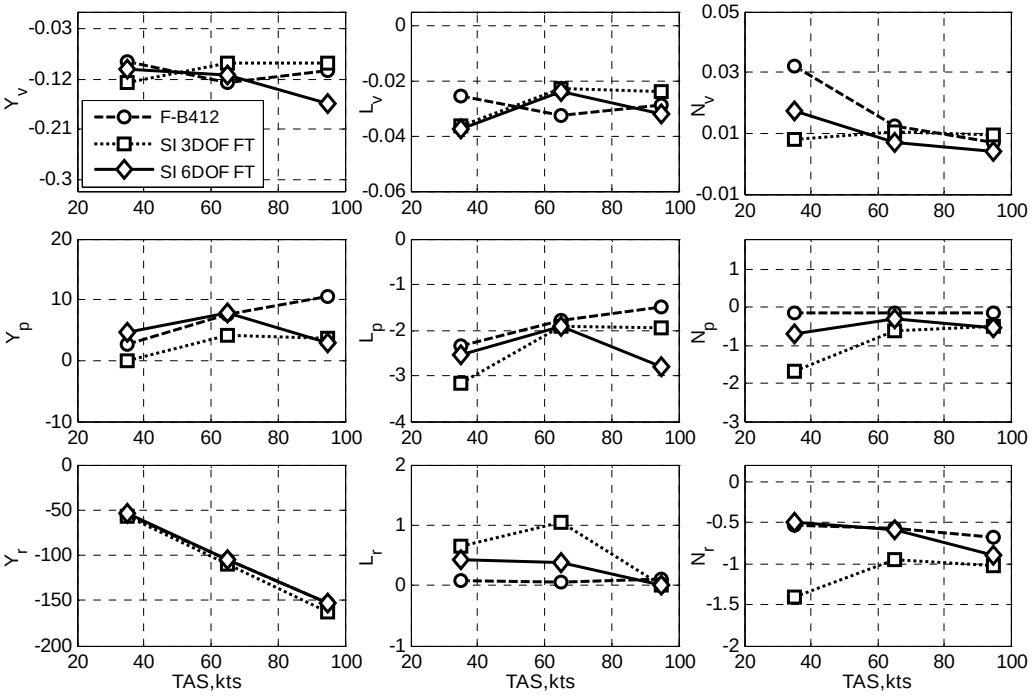

Figure 15 Comparison of longitudinal control derivatives from 3DOF and 6DOF SI FT and FLIGHTLAB perturbation

The key damping derivatives M_q, Y_v, L_p, and N_r in Figure 14 and Figure 15 match reasonably well and show broadly similar trends with forward speed; the same is true for the primary control derivatives $Z_{\delta_{lon}}$, $Z_{\delta_{col}}$ and $L_{\delta_{lat}}$. The cross-damping derivatives predicted by the 6 DoF SI generally compare poorly with the F-B412. The differences between the 'static' stability parameters M_w and N_v suggests that the F-B412 is more stable than the real aircraft. The forward speed damping derivative X_u has been eliminated or fixed in the identification model structure due to the lack of information content at low frequency. The heave damping derivative Z_w, and the yaw damping N_r, are expected to increase with forward speed over the range considered - approximately linearly up to moderate speeds and then levelling off at high speed [1].

The speed stability derivative M_u at 35 kts in Figure 14 is negative, exhibiting static speed instability for all sources, with increasing as speed increases for the SI results. However, the perturbation result increases positively with airspeed. This derivative is associated with the differential effects on advancing and retreating blades leading to flap back, and contributes to the dynamic phugoid instability.

The time-response verification, and significance of the differences, can be assessed by driving the models with the multi-step inputs. A selection of results showing the longitudinal and lateral channels from the 95 kts case, are plotted in Figure 16 and Figure 17.

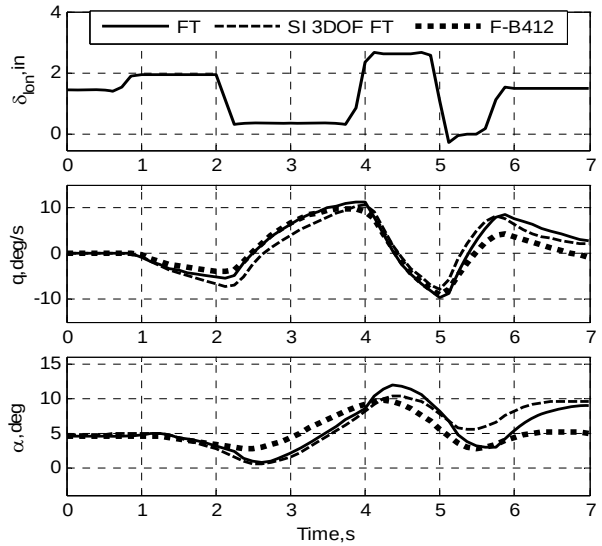

Figure 16 Verification of 3 DoF longitudinal dynamics at TAS = 95 kts and comparison with F-B412 responses

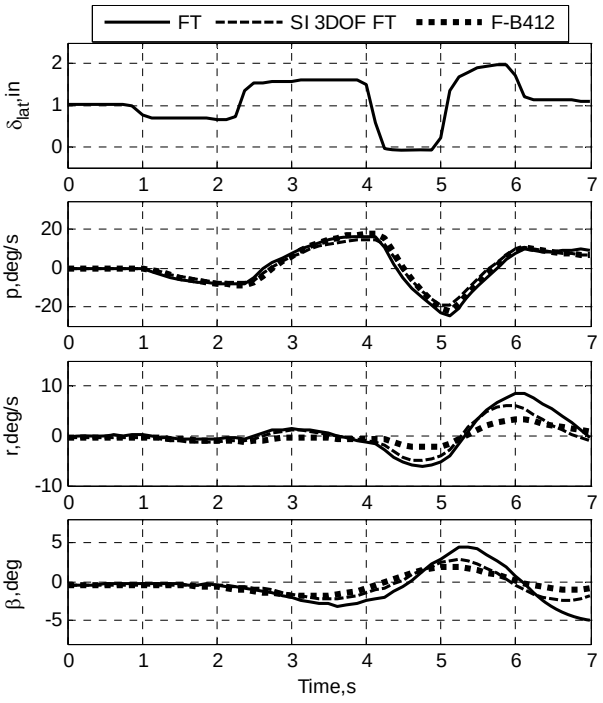

Figure 17 Verification of 3 DoF lateral-directional dynamics at TAS = 95 kts and comparison with F-B412 responses

The predictive capability of the SI models in the short term is very good; the match of incidence and sideslip is degrading at the end of the runs however. The SI flight-test model is more accurate than the F-B412; unsurprisingly as the parameters have been optimised to match the flight results over a similar frequency range. The F-B412 models fail to capture the initial response of the angle of attack following the longitudinal cyclic input and the sideslip response following the lateral cyclic input; results that are consistent with the mismatch of the static stability derivatives.

The static stability derivative M_w from the F-B412 is negative (stable), and positive (unstable) from flight test. As a first renovation exercise, Figure 18 shows results from the F-B412 model with the derivatives M_q and M_w replaced with the SI estimates. Changing the static stability on its own improves the incidence response over the first four seconds but degrades the pitch rate response.

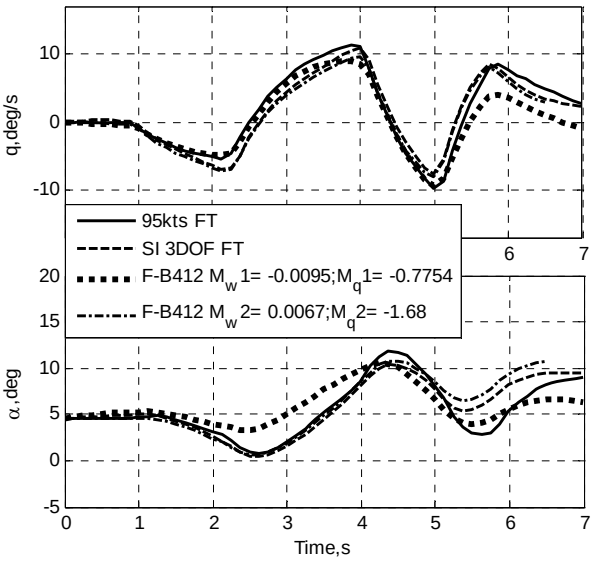

Figure 18 Response comparisons with renovated F-B412 model

There are three major components contributing to M_w − the main rotor (thrust offset and the hub moment), fuselage and tailplane. Their individual contributions to M_w for the F-B412 are roughly in the proportion +1, +4, −14, the tail therefore dominating the stabilising influence. Reducing the tailplane effectiveness would, however, reduce the damping. Further model renovation would need to examine the de-stabilising influences of the main rotor and fuselage.

A second renovation case examines the cross coupling between roll and yaw reflected in the derivative N_p, where the SI result is three time the magnitude of that predicted by F-B412. A comparison of roll and sideslip response is shown in Figure 19.

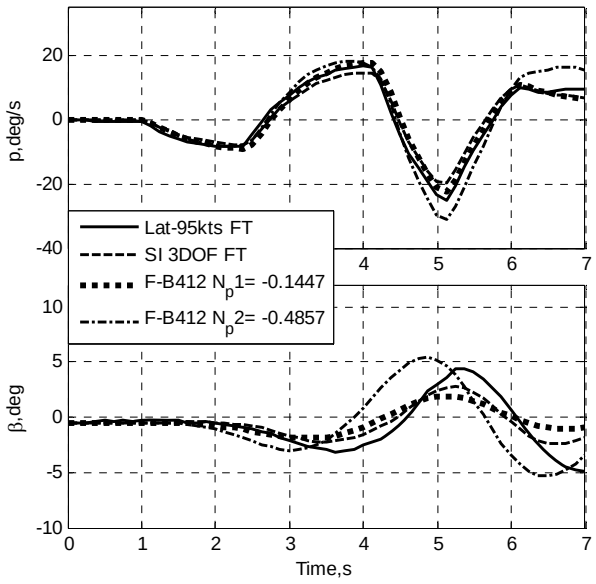

Figure 19 Response comparisons with Renovated F-B412 Model

The renovation has been partially successful in that the sideslip response now reaches similar levels to the flight data but the phase is wrong (hence phase of lateral acceleration cue to pilot) and the longer term roll rate response has been degraded. The derivative N_p is notoriously difficult to predict correctly, resulting from complex rotor torque variations during rolling manoeuvres. The directional stability is also over-predicted in the F-B412. Comparisons for the 6 DoF results are shown in Figure 20 and Figure 21.

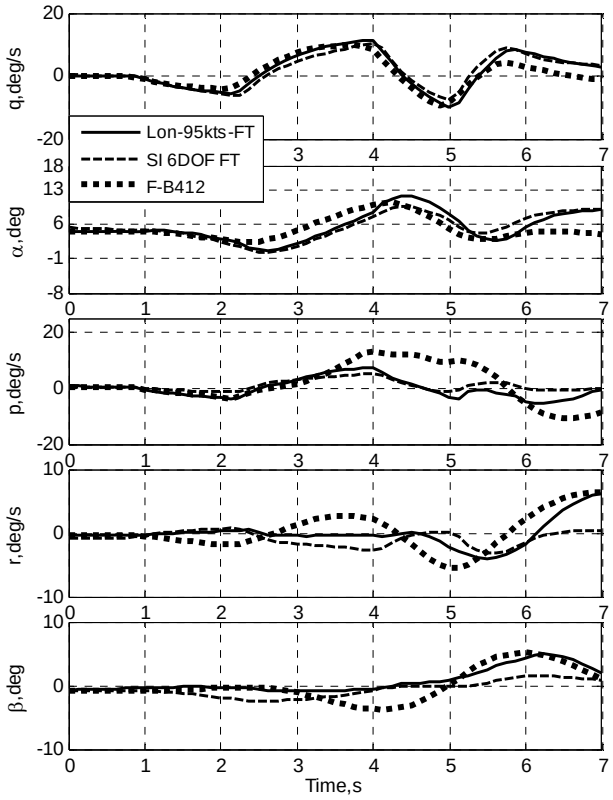

Figure 20 Verification of 6 DoF dynamics and comparison with F-B412, TAS = 95 kts, longitudinal control input

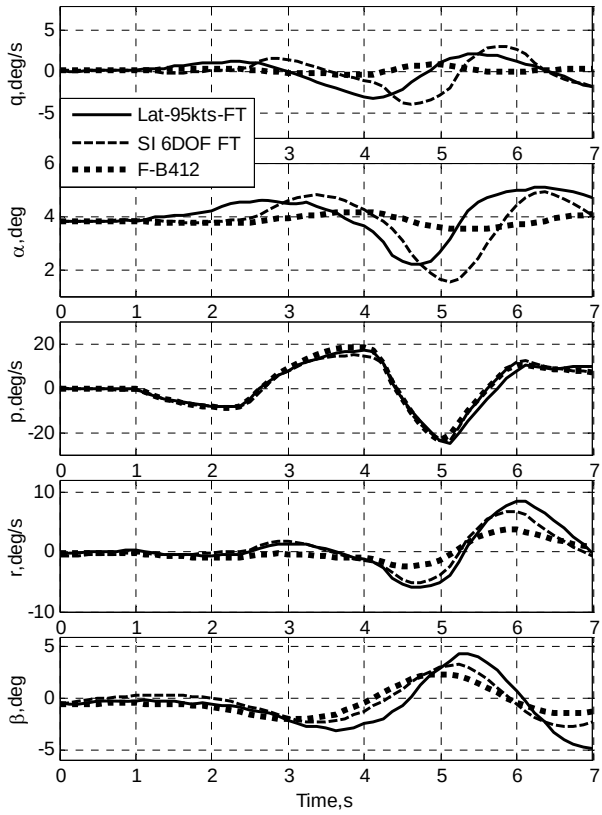

Figure 21 Verification of 6 DoF dynamics and comparison with F-B412, TAS = 95 kts, lateral control input

The on-axis responses for the 6 DoF model show similarly good agreement with flight test to the 3 DoF results. The off-axis responses – the roll/yaw/sideslip following the longitudinal cyclic input and, to a lesser extent, the pitch/incidence response to lateral cyclic – show a poorer agreement. Referring to the control derivatives in Appendix A, the pitching moment due to lateral cyclic ($M_{\delta_{lat}}$) is estimated to be 0.2 in flight and predicted as 0.035 in F-B412. Additionally, M_p is estimated to be -0.67 in flight and predicted to be 0.06 in F-B412, an order of magnitude increase. Both of these effects will contribute to the much reduced pitch response from lateral cyclic in the F-B412. However, as shown in Figure 22 the renovation of the F-B412 model through these two effects alone does not improve the off-axis response significantly. The cross damping derivative itself has increased the pitch response well beyond the level measured in flight.

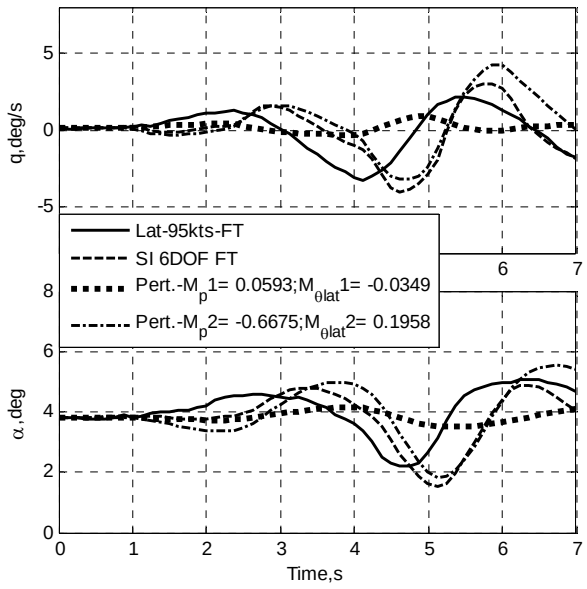

Figure 22 Comparison of pitch rate and incidence responses in renovated F-B412 Model

The roll and sideslip response to longitudinal cyclic is significantly over predicted in the F-B412 model. The cross damping effect L_q, deleted from the SI model through a poor CR fit, is strong in the F-B412 model (-0.93). The cross damping and control derivatives are strongly influenced by the wake distortion effects at low speed as discussed in Ref 16, but the influence is very small at 95 kts, accordingly to the FLIGHTLAB modelling.

In terms of stability, the combined effect of the differences in pitch damping and static stability is that the short period mode divides into two aperiodic modes in flight (-2.63, +0.319), while remaining an oscillation in the F-B412 (-0.972±1.2i). The combined effect of the differences in directional stability, roll damping and adverse yaw is that the Dutch roll is less stable in flight (-0.187±1.45i) than predicted for the F-B412 (-0.083±1.31i).

Renovation through model updating is more difficult with 6 DoF model structures and requires information on the sensitivity of response characteristics (in time and frequency domain) to the identified derivatives (flight data) and predicted derivatives (FLIGHTLAB). Such sensitivity analysis is being developed in the continuing research in the Lifting Standards project and will be reported at a future date.

CONCLUDING REMARKS

A frequency domain system identification methodology domain has been applied to evaluate the fidelity of the FLIGHTLAB F-B412 model. The results have shown that the identified model(s) compare well with flight test data over a range of forward speeds, based on frequency domain matching and verification using multi-step responses. The identified linear models thus serve as a good reference for renovating the F-B412 model.

The following conclusions and observations are drawn from this preliminary investigation;

1. The process of selecting and processing input-output transfer function pairs (the response fragments) for use in the CIFER® analysis provides a systematic and rational approach to the first stage of system identification. In some cases a wide frequency range can be included while in other only a narrow range conforms with the quality standards.
2. The model building from one, two, three and six degrees of freedom has been shown to be useful in providing references for model parameters, and can be used to guide parameter fixing. The use of an equivalent time delay has been shown to be effective in capturing the rotor dynamic effects.
3. The renovation process applied to the 3 DoF model identification has revealed how response mismatches can be 'repaired' through modifications to key F-B412 derivatives; e.g. the impact of M_w on incidence response to longitudinal cyclic and the impact of N_p on the sideslip response to lateral cyclic
4. In the case of the 6 DoF identification, the renovation process is considerably more complicated and examples have been shown where derivative changes have had both positive and negative results. A approach using sensitivity functions is required to develop a more systematic and rational approach to renovation.

This preliminary investigation has provided a basis for the continuing research, focusing on fidelity criteria and related enhancements for rotorcraft flight simulation.

ACKNOWLEDGEMENTS

The research reported in this paper is funded by the UK EPSRC through grant EP/G002932/1. The work also contributes to the University of Liverpool's Virtual Engineering Centre, supported by the European Regional Development Fund. The use of the Bell 412 ASRA facility is gratefully acknowledged, as is the support from Bill Gubbels, along with the flying expertise of Rob Erdos and Stephan Carignan, who were actively involved in the Phase 1 flight tests.

REFERENCES

[1] Padfield, G. D., *Helicopter Flight Dynamics,* 2nd ed., Blackwell Science, Oxford, 2007.

[2] Padfield, G. D., "Applications of System Identification in Rotorcraft Flight Dynamics," *Vertica*, Vol. 13, No. 3, 1989.

[3] AGARD, "Rotorcraft System Identification," AGARD AR 280, Sept. 1991.

[4] Klein, V., and Morelli, E. A., *Aircraft System Identification: Theory And Practice*, American Institute of Aeronautics & Astronautics, 2006.

[5] Tischler, M. B., and Remple, R. K., *Aircraft And Rotorcraft System Identification: Engineering*

Methods With Flight-test Examples, American Institute of Aeronautics & Astronautics, 2006.

[6] Padfield, G. D., and Du Val, R. W., "Application Areas of Rotorcraft System Identification - Simulation Model Validation," AGARD LS 178, Nov. 1991.

[7] Padfield, G. D., and White, M. D., "Measuring Simulation Fidelity Through An Adaptive Pilot Model," *Aerospace Science and Technology*, Vol. 9, May 2005, pp. 400-408.

[8] Padfield, G.D., Thorne, R., Murray-Smith, D. J., Black, C., Caldwell, A. E., "U.K. Research into System Identification for Helicopter Flight Mechanics," *Vertica*, Vol. 11, No. 4, 1987, pp. 665-684.

[9] Padfield, G.D., "SA 330 Puma Identification Results'. Lecture No. 10, AGARD Lecture Series No. 178: 'Rotorcraft system identification," AGARD, Neuilly-sur-Seine, France, 1991.

[10] Anon., *Handling Qualities Requirements for Military Rotorcraft*, US Army Aviation Command, ADS-33E-PRF, 2000.

[11] Zivan, L., Tischler, M.B., Development of a Full Flight Envelope Helicopter Simulation Using System Identification, *Journal of the American Helicopter Society*, 55, Apr. 2010, pp. 1-15.

[12] Drobik, J. S., and Brian, G. J., "Application of System Identification Techniques to the F-111C and PC 9/A Aircraft," *Journal of Aircraft*, Vol. 41, No. 4, Jul. 2004, pp. 744-751.

[13] Field, E. J., Rossitto, K. F., and Hodgkinson, J., "Flying Qualities Applications of Frequency Responses Identified From Flight Data," *Journal of Aircraft*, Vol. 41, No. 4, Jul. 2004, pp. 711-720.

[14] Morelli, E. A., and Klein,V., "Application of System Identification to Aircraft at NASA Langley Research Center," *Journal of Aircraft*, Vol. 42, No. 1, Jan. 2005, pp. 12-25.

[15] Morelli, E. A., "Low Order Equivalent System Identification for the Tu-144LL Supersonic Transport Aircraft," *J Guid Contr Dynam*, Vol. 26, No. 2, Mar. 2003, pp. 354-362.

[16] Grauer, J., Conroy, J., Hubbard, Jr., Humbert, J., and Pines, D., "System Identification of a Miniature Helicopter," *Journal of Aircraft*, Vol. 46, No. 4, Jul. 2009, pp. 1260-1269.

[17] Manimala, B., Walker, D., and Padfield, G.D., "Rotorcraft Simulation Modelling and Validation for Control Law Design," *Aeronautical Journal*, Vol. 111, Feb. 2007, pp. 77-88.

[18] White, M. D., Perfect, P., Padfield, G.D., Gubbels, A. W., and Berrayman, A. C., "Acceptance Testing of a Rotorcraft Flight Simulator for Research and Teaching: the Importance of Unified Metrics," *35th European Rotorcraft Forum*, Hamburg, Germany, 2009.

[19] Anon., *JAR-STD 1H, Helicopter Flight Simulators*, Joint Aviation Authorities, Apr. 2001.

[20] Anon., *AC 120-63 Helicopter Simulator Qualification*, Federal Aviation Administration Advisory Circular, Nov. 1994.

[21] Padfield, G.D., Pavel, M. D., Casolaro, D., Roth, G., Hamers, G., and Taghizad, A., "Simulation Fidelity of Real-time Helicopter Simulation Models," *Proc. American Helicopter Society 61st Annual Forum*, Grapevine, TX, 2005.

[22] Strope, K., Borden, C., and Harding, J., "Verification and Validation ofa UH-60 FLIGHTLAB model in support of the UH-60M Limited UserTest," *Proc. American Helicopter Society 60th Annual Forum*, Baltimore, MD, 2004.

APPENDIX –A

Table 4 Comparison 3DOF and 6 DOF of SI stability derivatives with those of the F-B412

Stability derivatives	Flight Test						F-B412		
	3DOF			6DOF			6DOF		
	35 kts	65 kts	95 kts	35 kts	65 kts	95 kts	35 kts	65 kts	95 kts
X_u	0.0000[d]	0.0000[d]	0.0000[d]	-0.0024[f]	-0.0245	-0.0473[f]	-0.0024	-0.0269	-0.0473
X_w	0.1531	0.0467	0.0224	0.0399	0.0779	0.0347	0.0531	0.0831	0.1215
X_q	-7.7870	-13.1244	-7.3745	-11.2368	-13.2068	-3.4969	-2.8794	-7.6252	-10.4305
X_v	--	--	--	-0.0628	-0.0473	0.0000[d]	-0.0379	-0.0208	-0.0274
X_p	--	--	--	-0.8344	-4.4827	0.0000[d]	-1.7319	-1.7272	-1.7079
X_r	--	--	--	1.6690	3.0739	0.0000[d]	-0.4430	-0.5679	-0.6607
Z_u	-0.1276	0.0000[d]	0.4282	-0.1893	0.1519	0.1599	-0.1587	0.0178	0.0874
Z_w	-0.7879	-0.6505	-0.5319	-0.5777	-0.8109	-0.8479	-0.6526	-0.8234	-0.9726
Z_q	63.0975	111.4371	163.4769	65.2923	113.0904	186.4677	57.8182	106.2897	155.0360
Z_v	--	--	--	-0.1358	-0.0951	0.0000[d]	-0.0398	-0.0435	-0.1822
Z_p	--	--	--	-4.4972	4.6930	0.0000[d]	8.6986	7.6379	4.8040
Z_r	--	--	--	8.3300	0.0000[d]	0.0000[d]	2.3607	2.6030	2.8344
M_u	0.0000[d]	0.0000[d]	-0.0068	-0.0027	-0.0020	-0.0040	-0.0012	0.0053	0.0052
M_w	0.0035	0.0049	0.0067	-0.0075	0.0035	0.0084	-0.0018	0.0035	-0.0095
M_q	-0.8032	-0.9649	-1.6792	-0.5660	-0.8438	-1.7367	-0.8390	-0.8805	-0.7754
M_v	--	--	--	0.0123	0.0037	0.0000[d]	0.0061	0.0015	0.0000
M_p	--	--	--	0.4084	-0.0744	-0.6675	0.1082	0.0124	0.0593
M_r	--	--	--	-0.2134	-0.2655	0.0255[c]	0.0059	0.0162	0.0255
Y_u	--	--	--	0.0000[d]	0.0000	0.0000[d]	0.0079	-0.0042	-0.0021
Y_w	--	--	--	0.0543	-0.0470	0.0000[d]	0.0133	0.0054	0.0161
Y_q	--	--	--	0.0000[d]	6.6956	-3.0198	0.5562	-3.1470	-3.1235
Y_v	-0.1268	-0.0914	-0.0915	-0.1025	-0.1140	-0.1652	-0.0897	-0.1279	-0.1055
Y_p	0.0000[d]	4.0503	3.6260	4.5932	7.7434	2.8390	2.7351	7.6327	10.5500
Y_r	-56.7582	-109.4166	-163.2544	-54.0369	-105.6787	-153.5829	-56.0263	-105.0206	-153.6845
L_u	--	--	--	0.0079	-0.0064	0.0000[d]	0.0038	-0.0063	-0.0060
L_w	--	--	--	0.0504	0.0047	0.0133	0.0227	0.0200	0.0197
L_q	--	--	--	0.0000[d]	1.9104	0.0000[d]	-0.0407	-0.9193	-0.9316
L_v	-0.0365	-0.0227	-0.0240	-0.0375	-0.0240	-0.0320	-0.0258	-0.0329	-0.0288
L_p	-3.1573	-1.9328	-1.9441	-2.5341	-1.9039	-2.8022	-2.3344	-1.7712	-1.4807
L_r	0.6588	1.0463	0.0000[d]	0.4360	0.3844	0.0000[d]	0.0690	0.0580	0.0925
N_u	--	--	--	-0.0034	0.0063	0.0021	-0.0036	-0.0028	-0.0025
N_w	--	--	--	-0.0047	-0.0305	-0.0060	0.0011	-0.0025	-0.0034
N_q	--	--	--	0.0000	2.3598	0.7617	-0.7060	0.7655	0.7091
N_v	0.0077	0.0104	0.0095	0.0175	0.0068	0.0039	0.0321	0.0124	0.0070
N_p	-1.6964	-0.6265	-0.4857	-0.7043	-0.3240	-0.5583	-0.1491	-0.1335	-0.1447
N_r	-1.2126	-0.9612	-1.0248	-0.5087	-0.5908	-0.8999	-0.5312	-0.5675	-0.6770

[d]Deleted from model structure
[f]Fixed in model structure

Table 5 Comparison 3DOF and 6 DOF of SI control derivatives with those of the F-B412

Control Derivatives	Flight Test						F-B412		
	3DOF			6DOF			6DOF		
	35 kts	65 kts	95 kts	35 kts	65 kts	95 kts	35 kts	65 kts	95 kts
$X_{\delta_{lon}}$	0.8720	1.1980	1.3015	1.4271	0.9057	1.2621	-0.8796	-0.6618	-0.3650
$X_{\delta_{lat}}$	--	--	--	0.0000[d]	1.1919	0.0000[d]	0.0987	0.0373	0.0729
$X_{\delta_{col}}$	0.6282	0.4016	0.0000[d]	0.0000[d]	0.5063	4.0267	0.6789	0.9441	1.4421
$X_{\delta_{ped}}$	--	--	--	0.7868	-6.2238	0.0000[d]	0.0388	-0.0309	-0.0044
$Z_{\delta_{lon}}$	3.1753	4.6076	5.7163	3.2105	5.0399	8.4049	-0.7840	-2.2037	-4.4107
$Z_{\delta_{lat}}$	--	--	--	0.0000	1.2885	0.0000[d]	0.2177	0.4689	1.0620
$Z_{\delta_{col}}$	-9.5562	-11.7620	-11.8698	-10.1577	-14.3578	-9.8304	-8.1180	-10.1051	-11.9381
$Z_{\delta_{ped}}$	--	--	--	7.0599	-3.8731	0.0000[d]	0.0406	0.0489	0.1981
$M_{\delta_{lon}}$	-0.2560	-0.2900	-0.3647	-0.2359	-0.2539	-0.3831	0.2292	0.2236	0.2163
$M_{\delta_{lat}}$	--	--	--	-0.0802	-0.0167	0.1958	-0.0257	-0.0261	-0.0349
$M_{\delta_{col}}$	0.0832	0.2163	0.3015	0.1288	0.1764	0.2326	0.0906	0.0494	0.0961
$M_{\delta_{ped}}$	--	--	--	-0.0715	0.0822	0.0000[d]	-0.0024	-0.0012	-0.0016
$Y_{\delta_{lon}}$	--	--	--	-0.3897	0.0000[d]	0.0000[d]	0.0320	0.1700	0.1303
$Y_{\delta_{lat}}$	3.2566	2.4126	2.8387	2.4293	2.5780	2.8244	0.8770	1.1075	1.1535
$Y_{\delta_{col}}$	--	--	--	0.0000[d]	-0.5845	0.0000[d]	-0.1626	0.0073	0.1248
$Y_{\delta_{ped}}$	0.0000[d]	1.9681	0.0000[d]	0.0000[d]	0.7491	0.0000[d]	-1.2637	-1.5164	-1.6103
$L_{\delta_{lon}}$	--	--	--	-0.2513	-0.1354	-0.1607	0.1302	0.2062	0.2356
$L_{\delta_{lat}}$	0.8593	0.7379	0.8160	0.9527	0.7518	1.0369	0.7942	0.8388	0.8486
$L_{\delta_{col}}$	--	--	--	0.0000[d]	0.0000[d]	0.0000[d]	0.0200	0.1767	0.2342
$L_{\delta_{ped}}$	0.4119	0.9745	0.6024	0.2293	0.6405	0.0000[d]	-0.3045	-0.3580	-0.3813
$N_{\delta_{lon}}$	--	--	--	0.0000[d]	0.4131	0.1124	0.0599	0.0057	0.0169
$N_{\delta_{lat}}$	0.3694	0.1713	0.1990	0.2076	0.1875	0.1863	0.1301	0.0669	0.0750
$N_{\delta_{col}}$	--	--	--	0.2236	-0.2502	0.0737	0.1838	0.1338	0.1360
$N_{\delta_{ped}}$	-0.4664	-0.3177	-0.4907	-0.3735	-0.4267	-0.5402	0.4793	0.5434	0.6079
$\tau_{\delta_{lon}}$	0.0559	0.0760	0.0989	0.0699	0.0340	0.1147			
$\tau_{\delta_{lat}}$	0.0823	0.0875	0.0974	0.0946	0.0608	0.1122			
$\tau_{\delta_{col}}$	0.0000[d]	0.0438	0.0527	0.1221	0.0460	0.0896			
$\tau_{\delta_{ped}}$	0.0828	0.0972	0.0902	0.0936	0.0928	0.0833			
CF.	**$115_{(Lon)}$**	**$112_{(Lon)}$**	**$116_{(Lon)}$**	**152**	**121**	**135**			
	$97.3_{(L/D)}$	**$113_{(L/D)}$**	**$118_{(L/D)}$**						